Center-to-limb variation of the continuum intensity and linear polarization of stars with transiting exoplanets

Shchukina, N. G.; Trujillo Bueno, J.; Vasilyeva, I. E.; Frantseva, K. V.

Published in:
Kinematics and physics of celestial bodies

DOI:
10.3103/S0884591317040043

Publication date:
2017

ISSN 0884-5913, Kinematics and Physics of Celestial Bodies, 2017, Vol. 33, No. 4, pp. 166–179. © Allerton Press, Inc., 2017.
Original Russian Text © N.G. Shchukina, J. Trujillo Bueno, I.E. Vasilyeva, K.V. Frantseva, 2017, published in Kinematika i Fizika Nebesnykh Tel, 2017, Vol. 33, No. 4, pp. 29–50.

PHYSICS OF STARS AND INTERSTELLAR MEDIUM

Center-to-Limb Variation of the Continuum Intensity and Linear Polarization of Stars with Transiting Exoplanets

N. G. Shchukina[a], *, J. Trujillo Bueno[b, c], I. E. Vasilyeva[a], **, and K. V. Frantseva[d, e]

[a] *Main Astronomical Observatory, National Academy of Sciences of Ukraine, Kyiv, 03143 Ukraine*
[b] *Instituto de Astrofísica de Canarias, 38205 La Laguna, Tenerife, Spain*
[c] *Departamento de Astrofísica, Universidad de La Laguna, 38206 La Laguna, Tenerife, Spain*
[d] *SRON Netherlands Institute for Space Research, Groningen, The Netherlands*
[e] *Kapteyn Astronomical Institute, University of Groningen, The Netherlands*
**e-mail: shchukin@mao.kiev.ua*
***e-mail: vasil@mao.kiev.ua*

Received July 7, 2016

Abstract—The limb darkening and center-to-limb variation of the continuum polarization is calculated for a grid of one-dimensional stellar model atmospheres and for a wavelength range between 300 and 950 nm. Model parameters match those of the transiting stars taken from the NASA exoplanet archive. The limb darkening of the continuum radiation for these stars is shown to decrease with the rise in their effective temperature. For the $\lambda = 370$ nm wavelength, which corresponds to the maximum of the Johnson–Cousins UX filter, the limb darkening values of the planet transiting stars lie in a range between 0.03 and 0.3. The continuum linear polarization depends not only on the effective temperature of the star but also on its gravity and metallicity. Its value decreases for increasing values of these parameters. In the *UX* band, the maximum linear polarization of stars with transiting planets amounts to 4%, while the minimum value is approximately 0.3%. The continuum limb darkening and the linear polarization decrease rapidly with wavelength. At the *R* band maximum ($\lambda = 700$ nm), the linear polarization close to the limb is in fact two orders of magnitude smaller than in the *UX* band. The center-to-limb variation of the continuum intensity and the linear polarization of the stars with transiting planets can be approximated, respectively, by polynomials of the fourth and the sixth degree. The coefficients of the polynomials, as well as the IDL procedures for reading them, are available in electronic form. It is shown that there are two classes of stars with high linear polarization at the limb. The first one consists of cold dwarfs. Their typical representatives are HATS-6, Kepler-45, as well as all the stars with similar parameters. The second class of stars includes hotter giants and subgiants. Among them we have CoRoT-28, Kepler-91, and the group of stars with effective temperatures and gravities of approximately 5000 K and 3.5, respectively.

DOI: 10.3103/S0884591317040043

INTRODUCTION

The search and study of exoplanets is one of the successfully developing fields of modern astrophysics. At present, the vast majority of planetary systems have been discovered from the observations of stellar luminosity variations that occur during the transit of planets across the star's disk (so-called transit photometry method or transit method). The second greatest amount of exoplanets have been discovered by observations of spectral line Doppler shifts (Doppler method or radial velocity method) caused by rotation of the star and planet about the common center of mass. Both methods complement each other, which makes it possible to obtain sufficiently accurate information on the mass, size, and orbital parameters of exoplanets. Among other methods, we should also mention the transit timing, gravitational microlensing, direct imaging, and method of discovering planets near pulsars by detecting the variations in pulse regularity (pulsation timing). The use of the astrometric method, based on measuring the movement of the star in a tiny orbit under the gravitation influence of an orbiting planet, so far has resulted in the discovery of only one planetary system.

Currently, there is an active discussion of possibilities to discover or confirm the existence of planets by measuring the variations of linear polarization of continuum radiation from exoplanetary systems [31]. It is known that the radiation from the whole disk of a spherically symmetrical star is unpolarized. Any

symmetry breaking leads to a non-zero linear polarization in integration over the disk. Asymmetry can be caused by the following factors: a change in the star's shape due to its rotation or tidal interaction with a planet, magnetic spots on the star's disk, temperature variations on its surface, or an occultation of the star by a transiting planet. Another source of polarization is the scattering of the star's radiation by molecules, aerosols, and dust particles in the planetary atmosphere [50, 58].

Theoretical estimates [5] show that the first effect is negligibly small: the maximum value of the linear polarization P does not exceed 3×10^{-9} of the unpolarized continuum radiation. The presence of spots can cause polarization from 3×10^{-6} to 10^{-5} and even 10^{-4} [5, 36, 41, 63]. Estimates of polarization magnitude caused by temperature variations on the star's surface are currently obtained only for the case of a gray atmosphere. According to the data [27] for variable stars of the Mira type, it can reach several percent. Observational data on the polarization due to the star's radiation being scattered by the planetary atmosphere are only known for a few exoplanetary systems [4, 5, 41, 63]. It should be noted that these data are quite contradictory. The scatter of polarization amplitudes obtained by different authors reaches two orders of magnitude and lies within the interval between 2.2×10^{-6} and 2×10^{-4}. The first results of modeling of the occultation of G, K, M, and T dwarf stars by planets were published in 2005 by Carciofi and Magalhães [15]. These authors showed that the polarization signal, while remaining rather weak ($P = 10^{-5}$–10^{-6}), exceeds the errors of modern spectral polarimeters.

The current studies in the field of spectral polarimetry of exoplanetary systems are mainly being carried out in three directions. First of all, the creation of highly sensitive stellar spectral polarimeters capable of measuring the signal on the order of $P = 10^{-5}$–10^{-7}. It should be noted that the information on such instruments was first published by Kemp et al. [34] as early as in 1987. Among polarimeters successfully operating today, we should mention CHEOPS (Characterization of Exoplanets by Opto-Infrared Polarimetry and Spectroscopy) [20, 49], PlanetPol [32], POLISH (POLarimeter for Inclination Studies of High mass x-ray binaries/Hot jupiters) [64], and ZIMPOL (Zurich IMaging POLarimeter) [59]. The second direction in polarimetry of exoplanetary systems is the analysis of chemical composition and structure of planetary atmospheres [5, 50, 55, 56, 58, 65]. The third direction is modeling of luminosity and linear polarization curves during occultation that occurs when one or more planets transit over the disk of a host star [15, 22, 30, 36, 37]. The final goal of such a modeling is to predict possible spectral polarimetry effects of transiting planets depending on their radius, orbital inclination, and period of rotation around the star.

In order to calculate these curves, it is necessary to know how the intensity and linear polarization of continuum radiation change from the center to the limb of the star [15]. The effect of limb darkening can be taken into account using nonlinear dependence on the polar angle μ, found by Claret [18] from a one-dimensional modeling for a large grid of wavelengths, effective temperatures, gravity, and metallicity. The other option is to use the limb darkening coefficients obtained by Sing [54] for the case of broadband filters onboard the CoRoT and Kepler space missions.

Until recently, the center-to-limb variation of linear polarization was typically described using the solar data calculated for one-dimensional [21] or three-dimensional model solar atmospheres [62] as well as using the Chandrasekhar approximation [17]. It should be noted that this approximation may yield large errors, since it is true only for O stars, whose main source of opacity is electron scattering. The stars with transiting planets are not of this type, since they belong to later spectral classes. According to Code [19] and Harrington [28], the joint action of Thompson scattering at electrons and absorption of continuum radiation by atoms in the atmospheres of such stars leads to a significant decrease in the linear polarization at the limb. For example, application of the Chandrasekhar approximation by Kostogryz et al. [37] to a star of spectral class K (HD 189733) yields polarization values overestimated by more than an order of magnitude.

This approach can be explained by the lack (until recently) of reliable data on the center-to-limb variation of the linear polarization of stars. A significant progress in this area occurred when N.G. Shchukina et al. [51–53], starting from 2013, presented the first results of modeling of limb darkening and continuum linear polarization for F, G, and K stars of various metallicity [Fe/H] in the wavelength range $\lambda = 300$–950 nm. In 2015, N.M. Kostogryz et al. [35, 36] published similar results for the stars with solar metallicity for the optical part of the spectrum ($\lambda = 400$–700 nm).

The objective of this paper is to present the results of calculations of the center-to-limb variation in intensity and linear polarization of continuum radiation for a grid of stellar model atmospheres, whose parameters match the stars with transiting planets discovered thus far.

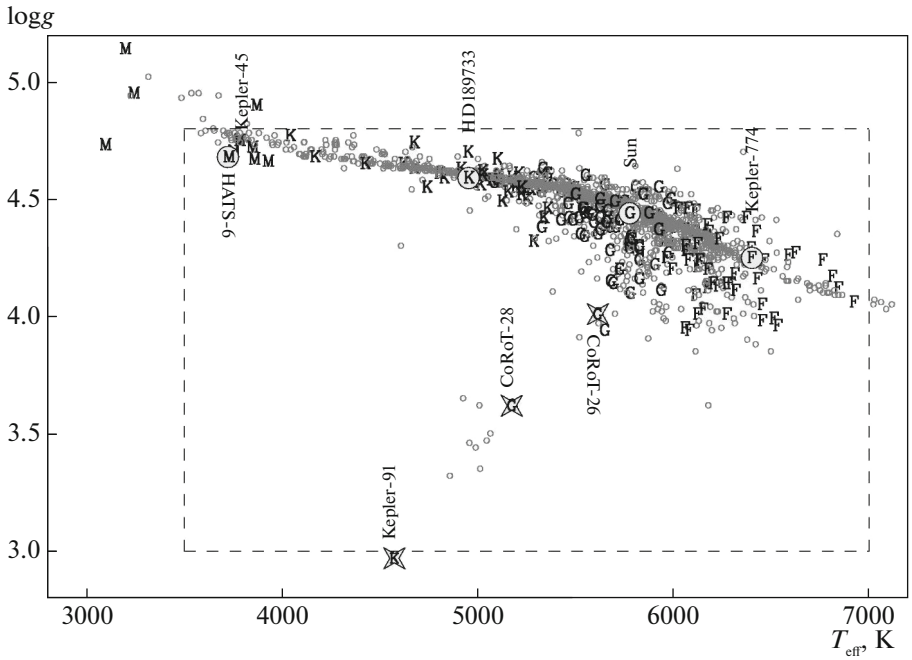

Fig. 1. Effective temperature–gravity diagram for stars with transiting planets. Letters M, K, G, and F denote the spectral classes of stars. Parameters of the stars are taken from the NASA archive http://exoplanetarchive.ipac.caltech.edu/corresponding to the period up to May 2016. The stars with no information on the spectral class in the NASA archive are marked with circles. The names are shown for typical stars with transiting planets (gray circles and asterisks) (see table). The rectangle inside the figure contains the stars with the parameter values in the range $4600 \le T_{\rm eff} \le 6400$ K and $3.0 \le \log g \le 4.8$.

STELLAR PARAMETERS OF TRANSIT SYSTEMS

We analyzed the stellar parameters of transit exoplanetary systems using the data from the NASA archive http://exoplanetarchive.ipac.caltech.edu/ corresponding to the period until May 2016. The archive contains information on planetary systems discovered by the space missions CoRoT (COnvection ROtation and planetary Transits) and Kepler as well as the ground-based programs of exoplanet search MEarth Project (searching for transiting habitable super-Earths around nearby M-dwarfs), HATNet (Hungarian Automated Telescope Network), SuperWASP (Wide Angle Search for Planets), OGLE (Optical Gravitational Lensing Experiment), KELT-South (Kilodegree Extremely Little Telescope), Trans-Atlantic Exoplanet Survey, etc.

Figure 1 shows the effective temperatures $T_{\rm eff}$ and gravity log$g$ for the stars with transiting planets from the abovementioned archive. By May 2016, the number of such stars had reached 1890. Where possible, we also mark the spectral classes of stars, denoting them by letters M, K, G, and F, correspondingly. The stars with no spectral class information in the NASA archive are marked with circles. Comparison of this figure with the Hertzsprung–Russell diagram [39] shows that most exoplanetary systems correspond to main-sequence stars. The number of stars evolved to the subgiant and giant stage is in fact two orders of magnitude lower.

The histograms of distribution of effective temperatures, gravity, and metallicity for the stars with transiting planets from the NASA archive are shown in Fig. 2. All of them have a distinct peak near solar values of $T_{\rm eff}$, log$g$, and [Fe/H]. For the vast majority of stars (>98%), their effective temperatures $T_{\rm eff}$ are within the range 3500–7000 K, and metallicity [Fe/H] is between –0.5 and +0.5. The number of stars with solar metallicity ($-0.1 \le$ [Fe/H] $\le +0.01$) is approximately 10%. The gravity values for almost all stars (99.3%) are within $3.0 \le \lg g \le 4.8$. The number of stars outside this range does not exceed 1%.

INPUT DATA AND METHOD

Model stellar atmospheres. Based on the above-mentioned statistics, we have modeled the center-to-limb variations of the continuum intensity and continuum linear polarization for a grid of one-dimensional model

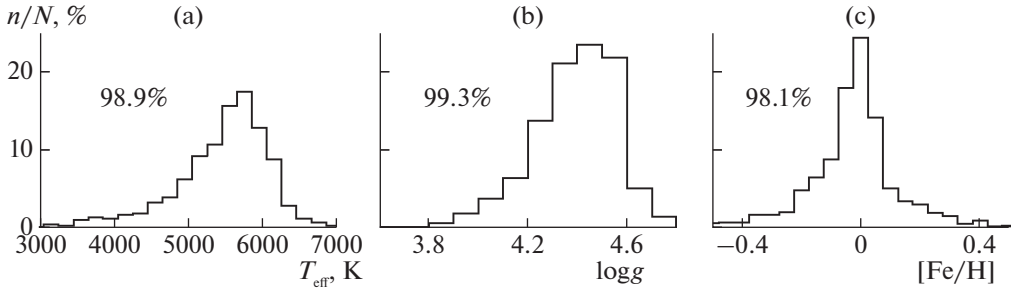

Fig. 2. Histograms of the values of effective temperature (a) $T_{\rm eff}$, (b) gravity log$g$, and (c) metallicity [Fe/H] for the stars with transiting planets. The data are taken from the NASA exoplanet archive. The numbers in the figure show the amount of stars (in % to the total number) in the intervals $4600 \le T_{\rm eff} \le 6400$ K, $3.0 \le \log g \le 4.8$, and $-0.5 \le$ [Fe/H] $\le +0.5$.

atmospheres by Kurucz [38] with the following stellar parameters: $3500 \le T_{\rm eff} \le 7000$ K, $3.0 \le \log g \le 4.8$, and $-0.5 \le$ [Fe/H] $\le +0.5$.

In calculating the continuum absorption coefficient, the following opacity sources were taken into account: bound–free and free–free absorption by hydrogen atoms (H^- and H I), bound–free absorption by metals (C, Mg, Al, Si, Fe), free–free absorption by H_2^+ molecules, Rayleigh scattering from the ground level of neutral hydrogen atoms, and Thompson scattering at electrons. We have also accounted for the "haze" opacity is formed in the spectral region at the wavelength $\lambda < 450$ nm. The "haze" was taken into account using the method described in [10].

Method. The polarized radiation is described by four Stokes parameters: I, Q, U, and V. In our calculations, we chose the reference frame where the Stokes parameter Q represents the linear polarization in the direction parallel to the stellar limb. This means that the second linear polarization parameter U turns to zero. The parameter of circular polarization V also equals zero, since we use the assumption that the magnetic field in the atmospheres of the stars under consideration is absent.

The numerical solution of transfer equations for the Stokes parameters I and Q was carried out using the iterative method developed for a one-dimensional case by Trujillo Bueno and Manso Sainz [61] as well as the NATAJA code based on this method. The details of this solution can be found in [62]. For the grid of model stellar atmospheres described above, we calculated the continuum intensity $I(\mu,\lambda)/I(\mu = 1,\lambda)$ (so-called limb darkening) and linear polarization $P(\mu,\lambda) = Q(\mu,\lambda)/I(\mu,\lambda)$ relative to the disk center intensity for different positions at the disk with a step $\Delta\mu = 0.025$. Here, $\mu = \cos\theta$, where θ is the angle between the direction of radiation and the normal to the surface of the atmosphere. The modeling of darkening and polarization of continuum radiation was performed for the wavelength interval $\lambda = 300$–950 nm with a variable step $\Delta\lambda$ changing from 5 nm to 20 nm in the infrared part of the spectrum.

RESULTS FOR THE GRID OF MODEL STELLAR ATMOSPHERES

The limb darkening of the continuum radiation intensity. The temperature of the outer layers of the stellar atmosphere (photosphere) rises with depth, which is known [43] to cause visible darkening of the disk's limb: while the optical length of the path is the same, the radiation in the center of the disk comes from deeper and, therefore, from hotter layers of the photosphere, unlike the radiation of the disk's periphery that comes at a tangent from cooler upper layers of the photosphere. The second effect that changes the magnitude of darkening is the dependence of the absorption coefficient on wavelength. In the wavelength range $\lambda = 300$–900 nm, the absorption of radiation by negative hydrogen ions, which is one of the continuous opacity sources in the atmospheres of the stars in our study, increases with wavelength (see, for example, Figs. 6 and 7 in the monograph by Sobolev [2]). As a result, the optical length of the continuum radiation path in the near infrared part of the spectrum is smaller, and the continuum formation region is higher than in the violet region (see Fig. 6 in [62]). Since the temperature gradient decreases with height, the stellar disks near the limb would appear brighter with increasing wavelength.

Figure 3 shows the ratio $I(\mu = 0.1)/I(\mu = 1)$ of the continuum radiation intensity at a distance $\mu = 0.1$ from the center of the disk to the intensity in the center ($\mu = 1$) calculated for the above-mentioned grid of stellar models depending on the effective temperature $T_{\rm eff}$, gravity log$g$, and metallicity [Fe/H]. The results in this figure are calculated for the wavelength $\lambda = 370$ nm corresponding to the maximum photometric passband UX in the Johnson–Cousins UVBRI system [6]. We shall note that this maximum is

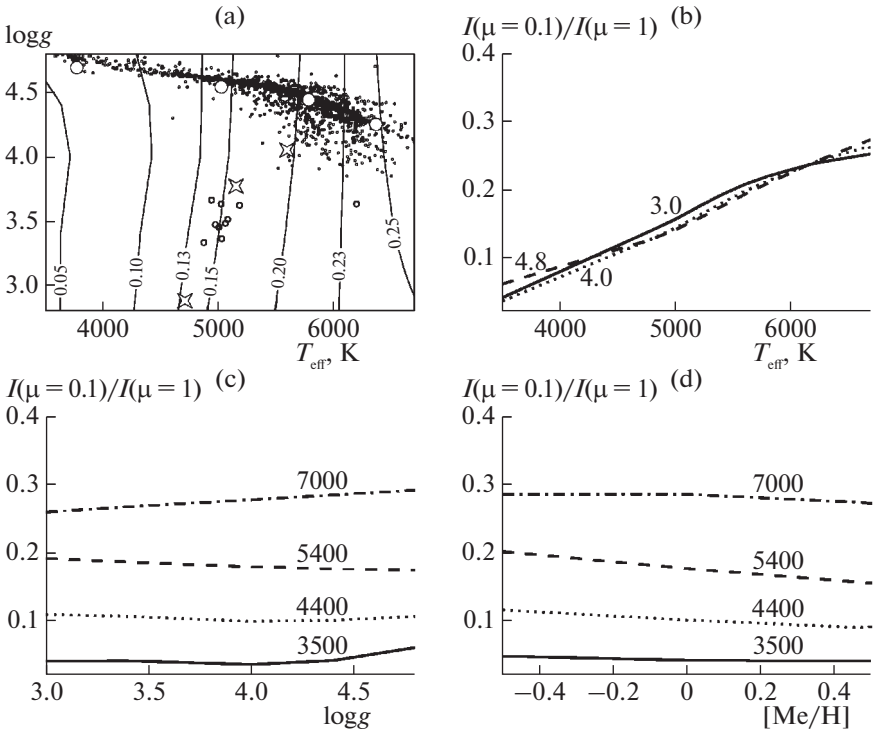

Fig. 3. Limb darkening $I(\mu = 0.1)/I(\mu = 1)$ calculated for the grid of model stars at $\lambda = 370$ nm (see text): (a) isolines of equal darkening for the stars with solar metallicity ([Fe/H] = 0.0) as a function of $T_{\rm eff}$ and log$g$ (the corresponding values of $I(\mu = 0.1)/I(\mu = 1)$ are shown at the isolines; the circles and asterisks mark the values for the stars from the NASA exoplanet archive); (b) dependences of darkening on the effective temperature for the stars with solar metallicity for three values log$g$ = 3.0, 4.0, and 4.8 (numbers at the curves); (c) dependences of darkening on gravity of the stars with solar metallicity for four values $T_{\rm eff}$ = 3500, 4400, 5400, and 7000 K; (d) dependences of darkening on stellar metallicity for the same four values of $T_{\rm eff}$ and gravity log$g$ = 4.4.

located just above the Balmer series boundary ($\lambda = 364.6$ nm). Our calculations for this model grid show that the ratio $I(\mu = 0.1)/I(\mu = 1)$ at this wavelength is several times lower than in the long-wave part of the spectrum ($\lambda = 950$ nm).

The isolines of constant values of darkening $I(\mu = 0.1)/I(\mu = 1)$ (excluding the regions of low and high effective temperatures) in Fig. 3a are almost parallel to the vertical axis of log$g$, which indicates the weak dependence of darkening on gravity; while, the limb brightness increases with the rise of the effective temperature. On the whole, at the wavelength $\lambda = 370$ nm, the values $I(\mu = 0.1)/I(\mu = 1)$ for the stars with transiting planets from the NASA archive lie within the range between 0.03 and 0.3. The results shown in Figs. 3b–3d provide a more detailed view on the dependence of the limb darkening in the UX band on the effective temperature, gravity, and metallicity of stars. It can be seen that the ratio $I(\mu = 0.1)/I(\mu = 1)$ for hot stars ($T_{\rm eff}$ = 7000 K) is at least five times higher than that for cool stars ($T_{\rm eff}$ = 3500 K). The limb brightness of hot stars weakly increases with lg$g$, while this dependence for cool stars is manifested only at log$g$ > 4.4. In the range –0.5 < [Fe/H] < +0.5, the limb darkening only slightly depends on metallicity.

Center-to-limb variations of the linear polarization of continuum radiation. Figure 4 shows the results of modeling the linear continuum polarization $Q(\mu = 0.1)/I(\mu = 0.1)$ near the limb ($\mu = 0.1$) at the wavelength $\lambda = 370$ nm for the grid of model stars considered above. The isolines shown in Fig. 4a significantly deviate from the vertical, indicating that the linear polarization, unlike the limb darkening, depends not only on the effective temperature but also on the gravity at the star's surface. Our calculations of $Q(\mu = 0.1)/I(\mu = 0.1)$ for the passbands V ($\lambda = 530$ nm) and R ($\lambda = 700$ nm) show that the isolines at other wavelengths behave in a similar way. From Figs. 4b and 4c, it can be seen that the linear polarization rapidly decreases with the rise of the effective temperature and gravity. For cool stars ($T_{\rm eff}$ = 3500 K) with log$g$ = 3.0, the linear polarization $Q(\mu = 0.1)/I(\mu = 0.1)$ exceeds 10%, while it is an order of magnitude less for hot stars ($T_{\rm eff}$ = 7000 K) with log$g$ = 4.8. The maximum linear polarization of stars with transiting planets from the NASA archive is approximately 4%, while the minimum value is approximately 0.3%. The dependence of the linear polarization on metallicity in the range of [Fe/H] between –0.5 and +0.5 is significantly weaker than on $T_{\rm eff}$

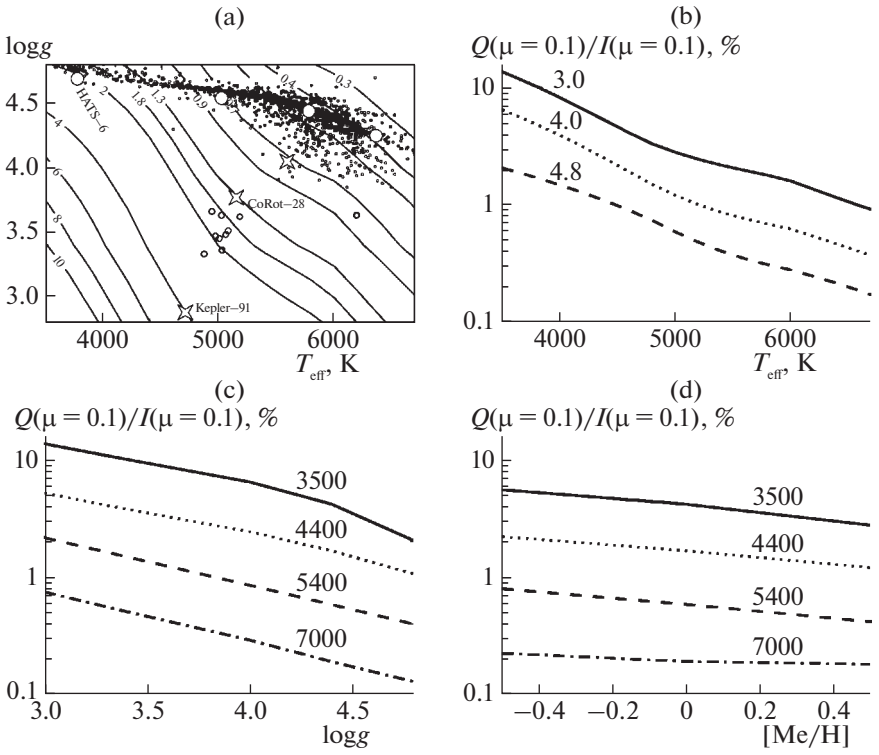

Fig. 4. Same for linear polarization $Q(\mu = 0.1)/I(\mu = 0.1)$.

and logg (Fig. 4d). The sensitivity of $Q(\mu = 0.1)/I(\mu = 0.1)$ to metallicity decreases with a rise in the effective temperature. The maximum effect is observed for cool stars ($T_{\rm eff} = 3500$ K). With the rise of metallicity in this range, the linear polarization reduces by approximately one half.

Approximate solution for linear polarization. The dependences of the linear continuum polarization on stellar parameters shown in Fig. 4 can be explained using the approximate expression for estimating the amplitude of the linear polarization of the emergent radiation $P(\mu,\lambda) = Q(\mu,\lambda)/I(\mu,\lambda)$ obtained by Trujillo Bueno and Shchukina in [62]:

$$\frac{Q(\mu,\lambda)}{I(\mu,\lambda)} = \frac{3\sqrt{2}}{2}\left(1-\mu^2\right)\frac{\sigma_c}{\sigma_c + k_c}\alpha\frac{J_0^2}{J_0^0}, \quad (1)$$

where k_c is the coefficient of continuum radiation absorption by atoms; σ_c is the coefficient of absorption caused by the Rayleigh and Thompson scattering; J_0^0 is the average intensity of radiation; J_0^2 is the tensor describing the "anisotropy" of the radiation field or, in other words, the degree of difference between the radiation field in vertical and horizontal direction. All the values refer to the atmospheric region where the intensity of the emergent continuum radiation is formed at a given wavelength. In literary sources, the ratio $\sigma_c/(\sigma_c + k_c)$ is referred to as the effective polarizability, and J_0^2/J_0^0 ratio is known as the anisotropy factor. These values, same as multiplier α, are the functions of wavelength λ. The α values range between 4.06 ($\lambda = 370$ nm) and 2.34 ($\lambda = 800$ nm).

From Eq. (1), it follows that the linear polarization mainly depends on the product of two values: effective polarizability and anisotropy factor. We have calculated their values for the limb ($\mu = 0.1$) at the wavelength $\lambda = 370$ nm depending on the effective temperature and gravity. The results of calculations are shown in Figs. 5a and 5b as isolines along which the effective polarizability and anisotropy factor remain the same. It should be noted that in calculation of $\sigma_c/(\sigma_c + k_c)$ and J_0^2/J_0^0, the region of continuum formation was found based on the Eddington–Barbier approximation (see formula (2.53) in the monograph [42]).

According to the approximation, this region is identified with the height where the optical depth at the given wavelength $\tau_\lambda(\mu) = \mu$. It can be seen from Fig. 5a that the isolines of the effective polarizability are characterized by horizontal orientation, while the isolines of the anisotropy factor are characterized by

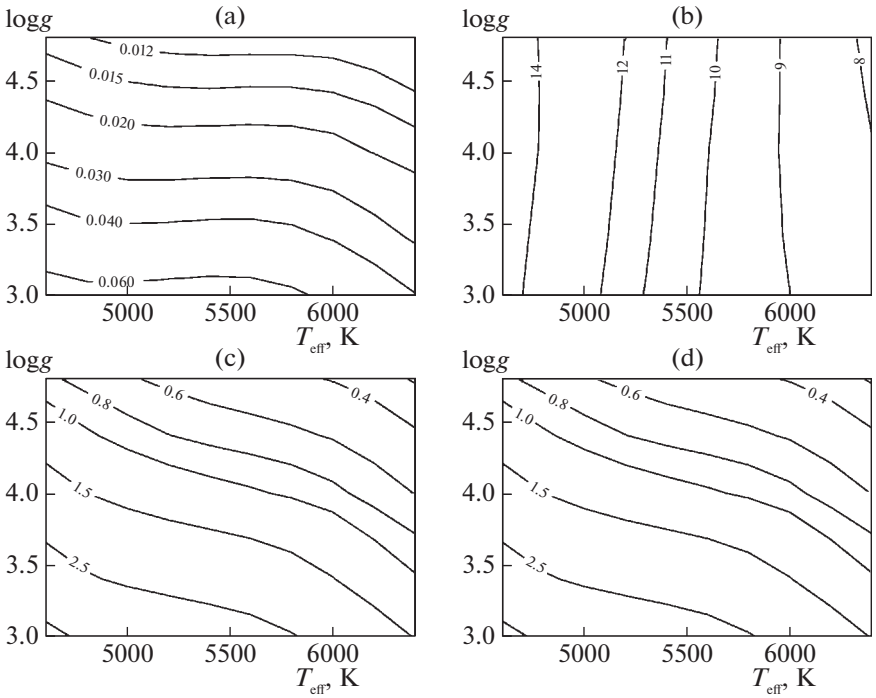

Fig. 5. Isolines of (a) effective polarizability $\sigma_c/(\sigma_c + k_c)$, (b) anisotropy factor J_0^2/J_0^0, and (c, d) linear polarization Q/I of the continuum radiation at the wavelength $\lambda = 370$ nm near the limb ($\mu = 0.1$), calculated as functions of two variables $T_{\rm eff}$ and lg$g$ for the stars with solar metallicity ([Fe/H] = 0); (c) approximate estimate of Q/I obtained using formula (1); (d) Q/I obtained by solving the transfer equations for Stokes parameters Q and I. All values are the functions of two variables: $T_{\rm eff}$ and log$g$. The values of $\sigma_c/(\sigma_c + k_c)$, J_0^2/J_0^0, and Q/I with corresponding isolines are shown in the figure.

vertical orientation. Such a behavior is the result of low sensitivity of $\sigma_c/(\sigma_c + k_c)$ to the effective temperature and high sensitivity to gravity. The anisotropy factor J_0^2/J_0^0, on the contrary, depends mainly on the effective temperature, and its value increases rapidly with decreasing $T_{\rm eff}$. As a result of combined action of these effects, the linear polarization of the emergent radiation becomes a function of two variables, namely, $T_{\rm eff}$ and log$g$.

Comparison of Figs. 5c and 5d shows that the approximate solution matches the solution found from the transfer equation for the polarized radiation with an accuracy to the coefficient α. Thus, approximation (1) is a sufficiently reliable estimate of the linear polarization for the stars of the considered grid provided that it is necessary to take into account into account not only the effective polarizability, like [35], but also the anisotropy factor.

Polynomial approximations of limb darkening and center-to-limb polarization of continuum radiation. Currently, there are a number of works published that suggest several kinds of approximations, from linear dependence to fourth-degree polynomial, for describing the center-to-limb dependence of stellar radiation intensity. The references to these works and the approximations themselves can be found in Claret's studies [18, 54]. In the present work, we have made an attempt to describe the limb darkening for the grid of model atmospheres as an analytical nonlinear dependence on μ. The results can be best represented with a fourth-degree polynomial, previously proposed by Claret:

$$\frac{I(\mu,\lambda)}{I(\mu=1,\lambda)} = D_0 + D_1 x + D_2 x^2 + D_3 x^3 + D_4 x^4, \qquad (2)$$

where

$$D_0 = 1 - D_1 - D_2 - D_3 - D_4, \quad x = \sqrt{\mu}.$$

To our knowledge, there are currently no publications where the variations of linear polarization from the center to the limb of the disk are presented as an analytical dependence on stellar parameters. In our

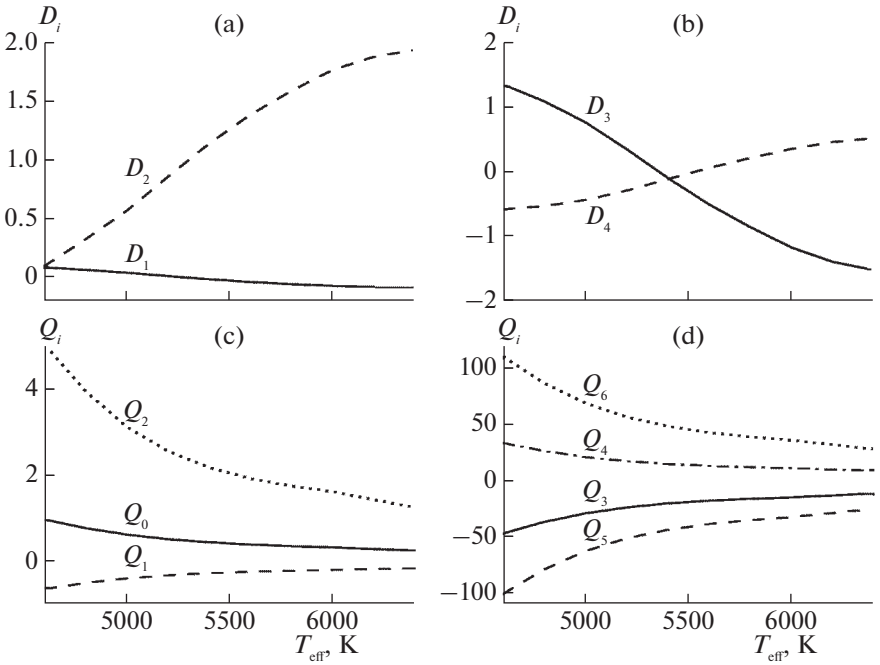

Fig. 6. Dependence of (a, b) coefficients D_i of polynomial approximation of limb darkening and (c, d) coefficients Q_i of polynomial approximation of center-to-limb linear polarization on the effective temperature of stars ($\lambda = 420$ nm, log$g = 4.4$, [Fe/H] = 0).

work, we have obtained such a dependence. It appears that, for our grid of stellar model atmospheres, the variation of the linear polarization over the stellar disk can be described with a sixth-degree polynomial:

$$\frac{Q(\mu,\lambda)}{Q(\mu,\lambda)} = Q_0 + Q_1 x + Q_2 x^2 + Q_3 x^3 + Q_4 x^4 + Q_5 x^5 + Q_6 x^6. \quad (3)$$

The coefficients D_i and Q_i are the functions of four variables: λ, $T_{\rm eff}$, log$g$, and [Fe/H]. The coefficients and IDL procedures for their reading are available in the electronic form. Figure 6, as an example, shows the dependence of these coefficients on the effective temperature for the case of solar metallicity [Fe/H] = 0, gravity log$g = 4.4$, and wavelength $\lambda = 420$ nm, which corresponds to the maximum photometric passband B in the Johnson–Cousins UVBRI system.

RESULTS FOR REPRESENTATIVE STARS WITH TRANSITING PLANETS

Characteristics of the representative stars with transiting planets. Above, we mainly discussed the behavior of darkening $I(\mu,\lambda)/I(\mu = 1,\lambda)$ and linear polarization $P(\mu,\lambda) = Q(\mu,\lambda)/I(\mu,\lambda)$ at the limb ($\mu = 0.1$) for a single wavelength. It is the most convenient to consider the dependences on the wavelength λ and position on the disk μ for typical samples of stars. From the set of stars with transiting planets shown in Figs. 1, 3a, and 4a, we have selected seven stars. Four of them (HATS-6, HD189733, Sun, and Kepler-774), marked with large circles, are located along the main sequence. The remaining three (CoRoT-26, CoRoT-28, and Kepler-91), marked with asterisks, are outside the main sequence. The stars and their parameters are listed in the Table 1. Taking into account that different methods of determining the stellar parameters lead to a large scatter in $T_{\rm eff}$, lg$g$, and [Fe/H] values, we list the minimum, average, and maximum values of these parameters. The calculations of the spectral energy distribution, limb darkening, and linear polarization for the stars from the table were carried out using the averaged values.

The exoplanetary system HD189733 is a binary star system: one component is a planet-hosting orange dwarf of spectral class K2V; the other one is a red M dwarf. The stars CoRoT-28 and CoRoT-26 (spectral classes G8/9 IV and G5) have left the main sequence and started evolving toward red giants, while Kepler-91 is already a red giant star of spectral class K3. The stars' masses are close to the solar mass, and their radii exceed the solar radius approximately by 2–6 times. The star of the orbiting planet Kepler-774 b, discovered in 2016, belongs to spectral class F and exceeds the solar mass by approximately 1.5 times. All the

Table 1. Parameters of the representative stars with transiting planets

Object	T_{eff}, K (min, mid, max)	log*g* (min, mid, max)	[Fe/H] (min, mid, max)	Reference
CoRoT-26	5590	3.99, 4.05, 4.10	+0.01	[3]
CoRoT-28	5150	3.60, 3.77, 3.94	+0.15	[14]
HD189733	4780, 5022, 5201	4.26, 4.54, 4.71	−0.37, −0.06, +0.13	[7, 9, 16, 23—26, 44, 46, 48, 57, 60, 66]
HATS-6	3722, 3773, 3872	4.68, 4.69, 4.69	+0.2	[29]
Kepler-91	4550, 4708, 4917	2.85, 2.88, 2.95	+0.11, +0.34, +0.51	[33, 40, 45, 47]
Kepler-774	6270, 6360, 6523	3.97, 4.25, 4.54	−0.43, −0.17, −0.08	[8, 11, 33, 45, 47]
Sun	5770	4.44	0.0	[1]

above-mentioned stars host at least one planet with an orbital period from 2 to 11 terrestrial days. All planets belong to the class of so-called hot Jupiters located close to the central star. The exoplanetary system HATS-6 consists of a dwarf star of spectral class M1 V and a Saturn-like planet with an orbital period of slightly more than 3 days. The mass and radius of the star are approximately half the Sun's.

Wavelength dependences of the continuum absolute intensity, limb darkening, and linear polarization. Figure 7a shows the spectral distribution of continuum radiation intensity $I(\mu,\lambda)$ in the center of the disk ($\mu = 1$) of representative stars for wavelengths between 300 and 950 nm. The behavior of the curves in this figure is in a full agreement with the assumption that the energy distribution with wavelength in these stars depends mainly on their effective temperature. The energy emitted by the hottest star Kepler-774 ($T_{\text{eff}} =$ 6360 K) exceeds the energy of the cool star Kepler-91 ($T_{\text{eff}} = 4708$ K) by several times. The calculated and observed [12, 13] distributions of intensity in the continuous spectrum of the Sun in Fig. 7a are in close agreement with each other, which indicates the reliability of the NATAJA code used in the numerical solution of the transfer equations for Stokes parameters *I* and *Q*.

The dependence of the limb darkening ($\mu = 0.1$) on T_{eff}, observed in the shortwave part of the spectrum in Fig. 3b, is also true for other wavelengths. It can be seen from Fig. 7b that, in the wavelength range $300 \le \lambda \le 950$ nm, the degree of limb darkening is reduced with wavelength for all types of the stars in question. In the near infrared part of the spectrum, corresponding to the maximum photometric passband $R(\lambda = 700$ nm) in the Johnson–Cousins system, the disk of the cool star Kepler-91 at the limb appears several times brighter than in the *UX* band. For the hot star Kepler-774, these differences are less: within a factor of 2. Figure 7c shows the results of modeling the linear polarization $P(\mu = 0.1,\lambda)$ of continuum radiation of representative stars near the limb ($\mu = 0.1$) depending on the wavelength. The linear polarization $P(\mu = 0.1,\lambda)$ at the limb, unlike the ratio $I(\mu = 0.1,\lambda)/I(\mu = 1,\lambda)$, rapidly decreases with wavelength. As can be seen it reaches maximum values in the shortwave part of the spectrum ($\lambda = 300$ nm). In the near infrared part of the spectrum ($\lambda = 700$ nm), the linear polarization at the limb is, in fact, two orders of magnitude less than in the UX band. Interestingly, the data presented in Fig. 7c do not correlate with the effective temperature. The reason for such a behavior of the linear polarization $P(\mu = 0.1,\lambda)$, as shown above, is that it depends not only on T_{eff} but also on the gravity.

The analysis of isolines in Fig. 4a calculated for the *UX* band leads to a conclusion that there are two classes of stars with a high polarization at the limb. The first class includes relatively cool dwarfs in the left upper corner of this figure (see also Fig. 1). Their typical representatives are HATS-6, Kepler-45, and all stars in Fig. 1 near them. This conclusion is in full agreement with the results of [36]. The second class of stars is hotter giants and subgiants that evolved away from the main sequence. It includes CoRoT-28, Kepler-91, and a group of stars in Fig. 4a between them. It can be seen from Fig. 7c that the linear polarization at the wavelength $\lambda = 300$ nm for the first of these stars is close to 4%, while that for the second one (Kepler-91) it reaches 10%.

Dependences of the limb darkening and linear polarization on position on the disk shown in Fig. 8 confirm a well-known fact that the darkening and linear polarization rapidly decrease toward the star's center [62]. This means that, in one-dimensional model atmospheres similar to the ones considered in this paper, in the center of the disk, $I(\mu,\lambda)/I(\mu = 1,\lambda) = 1$, and $P(\mu,\lambda) = 0$.

The intensification of darkening and polarization in transition to the shortwave part of the spectrum, clearly seen in Fig. 8, is in full agreement with the conclusions presented above. Interestingly, none of the stars in question, including HD 189733 mentioned in the Introduction, reach the values of $P(\mu,\lambda)$ pre-

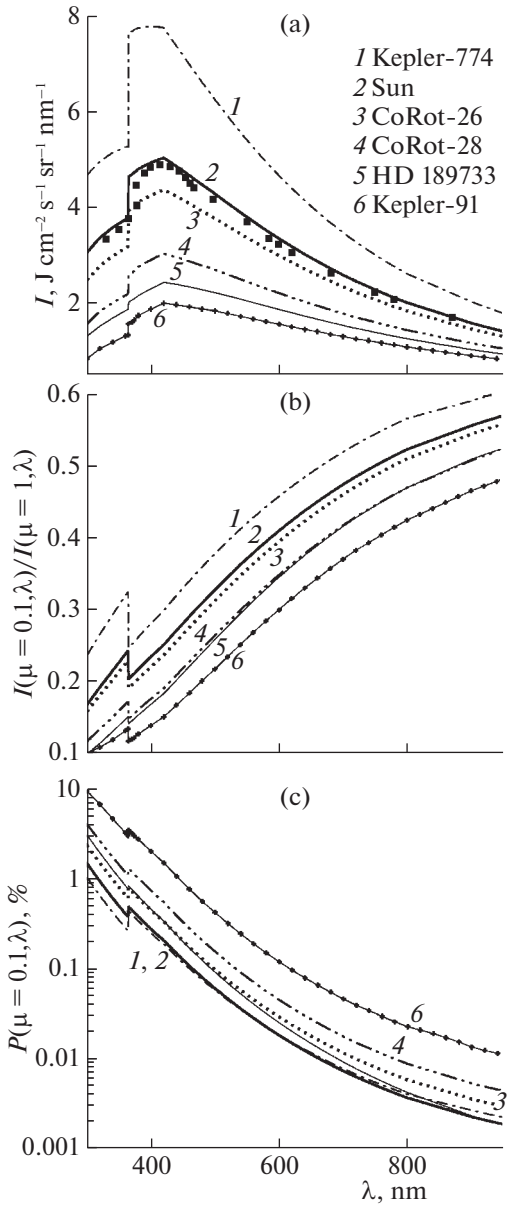

Fig. 7. Wavelength variation of (a) the continuum absolute intensity in the center of the disk, (b) limb darkening $I(\mu = 0.1,\lambda)/I(\mu = 1, \lambda)$, and (c) linear polarization $P(\mu = 0.1,\lambda)$ for the stars from the table. The squares mark the observational data [12, 13].

dicted by the Chandrasekhar approximation. In other words, this approximation is a strong overestimation of the linear polarization value in the stars with transiting planets and should be by all means avoided.

CONCLUSIONS

The main results of our study can be summarized as follows.

We have performed a modeling of center-to-limb variations of continuum intensity (limb darkening) and linear continuum polarization for the grid of one-dimensional model stellar atmospheres with the following parameters: $3500 \le T_{\rm eff} \le 7000$ K, $3.0 \le \log g \le 4.8$, and $-0.5 \le [{\rm Fe/H}] \le +0.5$. The analysis of the data from the NASA exoplanet archive for the period until May 2016 has shown that this range of effective temperature, gravity, and metallicity includes almost all stars with transiting planets (above 98%). Modeling of the darkening and polarization of continuum radiation was performed for the interval of wavelengths $\lambda = 300$–950 nm.

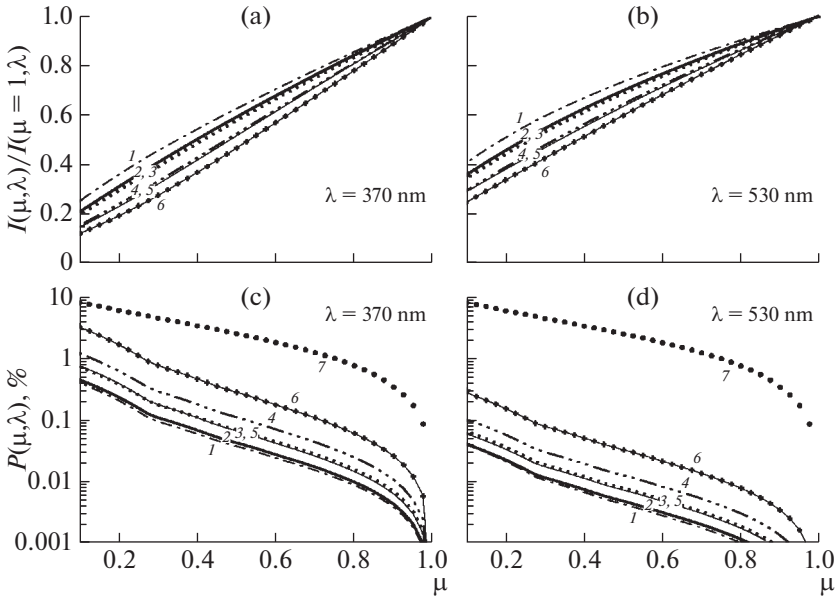

Fig. 8. Limb darkening (a, b) $I(\mu,\lambda)/I(\mu = 1,\lambda)$ and (c, d) linear polarization $P(\mu,\lambda)$ of the continuum radiation versus position at the stellar disk for the stars from the table (curve *7* is the Chandrasekhar approximation; see other notations in Fig. 7).

We have shown that, at an angular distance $\mu = 0.1$ from the center of the disk, the darkening rapidly decreases with increasing effective temperature of the star, while the dependence on gravity and metallicity is much weaker. On the whole, at the wavelength $\lambda = 370$ nm, the values of darkening for the stars with transiting planets from the NASA archive are between 0.03 and 0.3.

The linear polarization *P*, unlike the limb darkening, depends not only on the effective temperature of the star but also on its gravity. The *P* values decrease with increasing $T_{\rm eff}$ and log*g*. The dependence of the linear polarization on metallicity is weaker, and its sensitivity to this parameter reduces with an increase in effective temperature. With increasing metallicity, *P* values decrease by approximately two times. The maximum linear polarization of the stars with transiting planets from the NASA archive at the wavelength $\lambda = 370$ nm is 4%, while the minimum value is approximately 0.3%.

We have estimated the amplitude of the linear polarization of the emergent radiation using the approximation given by Trujillo Bueno and Shchukina in [62]. Comparison of the approximate solution with the accurate one obtained from the transfer equation for polarized radiation has shown that this approximation with an accuracy to the coefficient α is a reliable estimate of the linear polarization of stars with transiting planets.

We have described the limb darkening and linear polarization for the grid of model atmospheres as an analytical nonlinear dependence on $\mu^{1/2}$. It appears that the darkening is best represented with a fourth-degree polynomial and the linear polarization with a six-degree polynomial. The coefficients of the polynomials are the functions of four variables: λ, $T_{\rm eff}$, log*g*, and [Fe/H]. The coefficients and IDL procedures for reading them are available in electronic form.

We have discussed in detail the center-to-limb variations of intensity and linear polarization of several stars. From 1890 stars with transiting planets from the NASA archive, we have selected the most typical. These are HATS-6, HD189733, Kepler-774, CoRoT-26, CoRoT-28, and Kepler-91. We have shown that the spectral distribution of the continuum radiation intensity for these stars depends mainly on their effective temperature. In the wavelength range $\lambda = 300$–950 nm, the degree of limb brightness of stars with transiting planets increases, and linear polarization at the limb decreases with wavelength. In the near infrared part of the spectrum ($\lambda = 700$ nm), the linear polarization at the limb is in fact two orders of magnitude less than in the *UX* band ($\lambda = 370$ nm).

We have shown that there are two classes of stars with a high linear polarization at the limb. The first class includes relatively cool dwarfs. Their typical representatives are HATS-6, Kepler-45, and all stars with similar values of $T_{\rm eff}$, log*g*, and [Fe/H]. The second class consists of hotter giants and subgiants that evolved away from the main sequence. It includes CoRoT-28, Kepler-91, and a group of stars with effec-

tive temperature and gravity of approximately 5000 K and 3.5, respectively. The linear polarization in the ultraviolet at the wavelength $\lambda = 300$ nm for CoRoT-28 is close to 4%, while that for Kepler-91 reaches 10%. The dependences of the limb darkening and linear polarization on the position on the disk acquired in this work confirm the known fact that the darkening and linear polarization rapidly decrease toward the center of the star's disk. For all the stars under consideration, the P values are several times lower than predicted by the Chandrasekhar approximation. In other words, using this approximation to describe the linear polarization of stars with transiting planets is erroneous.

The results of this work can be used for predicting possible spectral polarimetry effects during transits of planets with different values of the radius, orbital inclination, and period of rotation around the star.

REFERENCES

1. C. W. Allen, *Astrophysical Quantities* (Athlone, London, 1973; Mir, Moscow, 1977).
2. V. V. Sobolev, *Course in Theoretical Astrophysics* (Nauka, Moscow, 1967; NASA, Washington, DC, 1969).
3. J. M. Almenara, F. Bouchy, P. Gaulme, et al., "Transiting exoplanets from the CoRoT space mission. XXIV. CoRoT-25b and CoRoT-26b: two low-density giant planets," Astron. Astrophys. **555**, A118 (2013).
4. S. V. Berdyugina, A. V. Berdyugin, D. M. Fluri, and V. Piirola, "First detection of polarized scattered light from an exoplanetary atmosphere," Astrophys. J. Lett. **673**, L83 (2008).
5. S. V. Berdyugina, A. V. Berdyugin, D. M. Fluri, and V. Piirola, "Polarized reflected light from the exoplanet HD189733B: First multicolor observations and confirmation of detection," Astrophys. J. Lett. **728**, L6 (2011).
6. M. S. Bessel, "UBVRI passbands," Publ. Astron. Soc. Pac. **102**, 1181–1199 (1990).
7. A. Bonfanti, S. Ortolani, and V. Nascimbeni, "Age consistency between exoplanet hosts and field stars," Astron. Astrophys. **585**, A5 (2016).
8. W. J. Borucki, D. G. Koch, G. Basri, et al., "Characteristics of planetary candidates observed by Kepler. II. Analysis of the first four months of data," Astrophys. J. **736**, 19 (2011).
9. F. Bouchy, S. Udry, M. Mayor, et al., "ELODIE metallicity-biased search for transiting Hot Jupiters. II. A very hot Jupiter transiting the bright K star HD 189733," Astron. Astrophys. **444**, L15–L19 (2005).
10. J. H. M. J. Bruls, "The formation of helioseismology lines. IV — The NI I 676.8 NM intercombination line," Astron. Astrophys. **269**, 509–517 (1993).
11. L. A. Buchhave, D. W. Latham, J. A. Carter, et al., "Kepler-14b: A massive hot Jupiter transiting an F star in a close visual binary," Astrophys. J., Suppl. Ser. **197**, 3–10 (2011).
12. K. A. Burlov-Vasiljev, E. A. Gurtovenko, and Yu. B. Matvejev, "New absolute measurements of the solar spectrum 310–685 nm," Sol. Phys. **157**, 51–73 (1995).
13. K. A. Burlov-Vasiljev, Yu. B. Matvejev, and I. E. Vasiljeva, "New measurements of the solar disk-center spectral intensity in the near IR from 645 nm to 1070 nm," Sol. Phys. **177**, 25–40 (1998).
14. J. Cabrera, Sz. Csizmadia, G. Montagnier, et al., "Transiting exoplanets from the CoRoT space mission. XXVII. CoRoT-28b, a planet orbiting an evolved star, and CoRoT-29b, a planet showing an asymmetric transit," Astron. Astrophys. **579**, A36 (2015).
15. A. C. Carciofi and A. M. Magalhães, "The polarization signature of extrasolar planet transiting cool dwarfs," Astrophys. J. **635**, 570–577 (2005).
16. L. Casagrande, R. Schönrich, M. Asplund, et al., "New constraints on the chemical evolution of the solar neighbourhood and Galactic disc(s). Improved astrophysical parameters for the Geneva–Copenhagen Survey," Astron. Astrophys. **530**, A138 (2011).
17. S. Chandrasekhar, "On the radiative equilibrium of a stellar atmosphere. X," Astrophys. J. **103**, 351–370 (1946).
18. A. Claret, "A new non-linear limb-darkening law for LTE stellar atmosphere models. Calculations for $-5.0 <= \log[M/H] <= +1$, $2000\ K <= T_{eff} <= 50000\ K$ at several surface gravities," Astron. Astrophys. **363**, 1081–1190 (2000).
19. A. D. Code, "Radiative equilibrium in an atmosphere in which pure scattering and pure absorption both play a role," Astrophys. J. **112**, 22–24 (1950).
20. M. Feldt, M. Turatto, H. M. Schmid, et al., ""Planet Finder" instrument for the ESO VLT," in *Proc. Towards Other Earths — DARWIN/TPF and the Search for Extrasolar Terrestrial Planets, Heidelberg, Germany. Apr. 22–25, 2003*, Ed. by M. Fridlund and T. Henning (Eur. Space Agency, Noordwijk, 2003), pp. 99–107.
21. A. D. Fluri, J. O. Stenflo, "Continuum polarization in the solar spectrum," Astrophys. J. **341**, 902–911 (1999).
22. K. Frantseva, N. M. Kostogryz, and T. M. Yakobchuk, "Simulation of polarimetric effects in planetary system HD 189733," Adv. Astron. Space Phys. **2**, 146–148 (2012).
23. K. Fuhrmann, "Nearby stars of the Galactic disc and halo — IV," Mon. Not. R. Astron. Soc. **384**, 173–224 (2008).

24. L. Ghezzi, K. Cunha, V. V. Smith, et al., "Stellar parameters and metallicities of stars hosting Jovian and Neptunian mass planets: A possible dependence of planetary mass on metallicity," Astrophys. J. **720**, 1290–1302 (2010).
25. G. Gonzalez, M. K. Carlson, and R. W. Tobin, "Parent stars of extrasolar planets — X. Lithium abundances and v sin i revisited," Mon. Not. R. Astron. Soc. **403**, 1368–1380 (2010).
26. R. O. Gray, C. J. Corbally, R. F. Garrison, et al., "Contributions to the nearby stars (NSTARS) project: Spectroscopy of stars earlier than M0 within 40 parsecs: The northern sample. I," Astron. J. **126**, 2048–2059 (2003).
27. J. P. Harrington, "The intrinsic polarization of Mira Variables," Astrophys. Lett. **3**, 165–168 (1969).
28. J. P. Harrington, "Polarization of radiation from stellar atmospheres. The grey case," Astrophys. Space Sci. **8**, 227–242 (1970).
29. J. D. Hartman, D. Bayliss, R. Brahm, et al., "HATS-6b: A warm Saturn transiting an early M dwarf star, and a set of empirical relations for characterizing K and M dwarf planet hosts," Astron. J. **149**, 166 (2015).
30. W. Hayek, D. Sing, F, Pont, and M. Asplund, "Limb darkening laws for two exoplanet host stars derived from 3D stellar model atmospheres. Comparison with 1D models and HST light curve observations," Astron. Astrophys. **539**, A102 (2012).
31. J. Hough, "Polarimetry: A powerful diagnostic tool in astronomy," Astron. Geophys. **47**, 3.31–3.35 (2006).
32. J. H. Hough, P. W. Lucas, J. A. Bailey, et al., "PlanetPol: A very high sensitivity polarimeter," Publ. Astron. Soc. Pac. **118**, 1302–1318 (2006).
33. D. Huber, V. Silva Aguirre, J. M. Matthews, et al., "Revised stellar properties of Kepler targets for the quarter 1-16 transit detection run," Astrophys. J., Suppl. Ser. **211**, 2 (2014).
34. J. C. Kemp, G. D. Henson, C. T. Steiner, and E. R. Powell, "The optical polarization of the Sun measured at a sensitivity of parts in ten million," Nature **326**, 270–273 (1987).
35. N. M. Kostogryz and S. V. Berdyugina, "Center-to-limb polarization in continuum spectra of F, G, K stars," Astron. Astrophys. **575**, A89–A97 (2015).
36. N. M. Kostogryz, T. M. Yakobchuk, and S. V. Berdyugina, "Polarization in exoplanetary systems caused by transits, grazing transits, and starspots," Astrophys. J. **806**, 97 (2015).
37. N. M. Kostogryz, T. M. Yakobchuk, O. V. Morozhenko, and A. P. Vid'machenko, "Polarimetric study of transiting extrasolar planets," Mon. Not. R. Astron. Soc. **415**, 695–700 (2011).
38. R. L. Kurucz, *ATLAS9 Stellar Atmospheres Programs and 2 km/s Grid*, Kurucz CD-ROM No. 13 (Smithson. Astrophys. Obs., Cambridge, MA, 1993).
39. K. R. Lang, *Astrophysical Formulae* (Springer-Verlag, Berlin, 1974), Ch. 9.
40. J. Lillo-Box, D. Barrado, A. Moya, et al., "Kepler-91b: a planet at the end of its life. Planet and giant host star properties via light-curve variations," Astron. Astrophys. **562**, A109 (2014).
41. P. W. Lucas, J. H. Hough, J. A. Bailey, et al., "Planetpol polarimetry of the exoplanet systems 55 Cnc and τ Boo," Mon. Not. R. Astron. Soc. **393**, 229–244 (2009).
42. D. Mihalas, *Stellar Atmospheres*, 2nd ed. (W. H. Freeman, San Francisco, 1978).
43. E. A. Milne, in *Handbuch der Astrophysik*, Ed. by G. Eberhard, A. Konlschüüter, and H. Ludendorff (Springer-Verlag, Berlin, 1930), Vol. 3, Part 1, p. 145.
44. T. V. Mishenina, M. Pignatari, S. A. Korotin, et al., "Abundances of neutron-capture elements in stars of the Galactic disk substructures," Astron. Astrophys. **552**, A128 (2013).
45. M. H. Pinsonneault, D. An, J. Molenda-Żakowicz, et al., "A revised effective temperature scale for the Kepler input catalog," Astrophys. J., Suppl. Ser. **199**, 30 (2012).
46. I. Ramirez, J. R. Fish, and D. L. Lambert, Allende Prieto C. "Lithium abundances in nearby FGK dwarf and subgiant stars: Internal destruction, galactic chemical evolution, and exoplanets," Astrophys. J. **756**, 46 (2012).
47. J. F. Rowe, J. L. Coughlin, V. Antoci, et al., "Planetary candidates observed by Kepler. V. Planet sample from Q1–Q12 (36 months)," Astrophys. J., Suppl. Ser. **217**, 16 (2015).
48. N. C. Santos, S. G. Sousa, A. Mortier, et al., "SWEET-Cat: A catalogue of parameters for stars with exoplanets. I. New atmospheric parameters and masses for 48 stars with planets," Astron. Astrophys. **556**, A150 (2013).
49. H. M. Schmid, D. Gisler, F. Joos, et al., "ZIMPOL/CHEOPS: A polarimetric imager for the direct detection of extra-solar planets," in *Proc. Astronomical Polarimetry: Current Status and Future Directions in Waikoloa, HI, Mar. 15–19, 2004*, Ed. by A. Adamson, C. Aspin, C. J. Davis, and T. Fujiyoshi (Astron. Soc. Pac., 2005), in Ser.: *ASP Conference Series*, Vol. 343, pp. 89–91.
50. S. Seager, B. A. Whitney, and D. D. Sasselov, "Photometric light curves and polarization of close-in extrasolar giant planets," Astrophys. J. **540**, 504–520 (2000).
51. N. G. Shchukina, K. V. Frantseva, and J. Trujillo Bueno, "The continuum polarization of stars with transiting exoplanetary systems," Presented at WG1 Meeting: Polarimetry of Planetary Systems (COST Action MP1104 — Polarisation as a Tool to Study the Solar System and Beyond), Florence, Italy, Sept. 23–27, 2013. http://www.polarisation.eu/index.php/meetings/previous-meetings/10-meetings/102-polarimetry-planetary-systems.

52. N. G. Shchukina, K. V. Frantseva, and J. Trujillo Bueno, "Continuum polarization of stars as a result of occultation by transiting exoplanets," in *Proc. 21th Young Scientists' Conf. on Astronomy and Space Physics, Kyiv, Ukraine, Apr. 28 – May 3, 2014* (Kyiv. Nats. Univ. im. Tarasa Shevchenka, Kyiv, 2014), p. 12. http://ysc.kiev.ua.
53. N. G. Shchukina, K. V. Frantseva, and J. Trujillo Bueno, "Continuum polarization of stars as a result of occultation by transiting exoplanets," Presented at WG2 Meeting: Theory and Modeling of Polarisation in Astrophysics (COST Action MP1104 — Polarisation as a Tool to Study the Solar System and Beyond), Prague, Czech, May 5–8, 2014. http://www.asu.cas.cz/~wg2prague/talks.html.
54. D. K. Sing, "Stellar limb-darkening coefficients for CoRot and Kepler," Astron. Astrophys. **510**, A21 (2010).
55. D. K. Sing, J-M. Désert, J. J. Fortney, et al., "Gran Telescopio Canarias OSIRIS transiting exoplanet atmospheric survey: Detection of potassium in XO-2b from narrowband spectrophotometry," Astron. Astrophys. **527**, A73 (2011).
56. D. K. Sing, J-M. Désert, A. Lecavelier des Etangs, et al., "Transit spectrophotometry of the exoplanet HD 189733b. I. Searching for water but finding haze with HST NICMOS," Astron. Astrophys. **505**, 891–899 (2009).
57. S. G. Sousa, N. C. Santos, G. Israelian, et al., "Spectroscopic parameters for a sample of metal-rich solar-type stars," Astron. Astrophys. **458**, 873–880 (2006).
58. D. M. Stam, J. W. Hovenier, L. B. F. M. Waters, "Using polarimetry to detect and characterize Jupiter-like extrasolar planets," Astron. Astrophys. **428**, 663–672 (2004).
59. J. O. Stenflo, C. U. Keller, and A. Gandorfer, "Anomalous polarization effects due to coherent scattering on the Sun," Astron. Astrophys. **355**, 789–803 (2000).
60. G. Torres, D. A. Fischer, A. Sozzetti, et al., "Improved spectroscopic parameters for transiting planet hosts," Astrophys. J. **757**, 161 (2012).
61. J. Trujillo Bueno and R. Manso Sainz, "Iterative methods for the non-LTE transfer of polarized radiation: Resonance line polarization in one-dimensional atmospheres," Astrophys. J. **516**, 436–450 (1999).
62. J. Trujillo Bueno and N. G. Shchukina, "Three-dimensional radiative transfer modeling of the polarization of the Sun's continuous spectrum," Astrophys. J. **694**, 1364–1378 (2009).
63. S. J. Wiktorowicz, "Nondetection of polarized, scattered light from the HD 189733b hot Jupiter," Astrophys. J. **696**, 1116–1124 (2009).
64. S. J. Wiktorowicz and K. A. Matthews, "A high-precision optical polarimeter to measure inclinations of high-mass X-ray binaries," Publ. Astron. Soc. Pac. **120**, 1282–1297 (2008).
65. P. A. Wilson, K. D. Colón, D. K. Sing, et al., "A search for methane in the atmosphere of GJ 1214b via GTC narrow-band transmission spectrophotometry," Mon. Not. R. Astron. Soc. **438**, 2395–2405 (2014).
66. N. J. Wright, J. J. Drake, E. E. Mamajek, and G. W. Henry, "The stellar-activity-rotation relationship and the evolution of stellar dynamos," Astrophys. J. **743**, 48 (2011).

Translated by M. Chubarova